Applied Catalysis B: Environmental 221 (2018) 339–348

Contents lists available at ScienceDirect

Applied Catalysis B: Environmental

journal homepage: www.elsevier.com/locate/apcatb

Research paper

Silver/Silver(II) oxide (Ag/AgO) loaded graphitic carbon nitride microspheres: An effective visible light active photocatalyst for degradation of acidic dyes and bacterial inactivation

Devthade Vidyasagar[a], Sachin G. Ghugal[a], Aditi Kulkarni[b], Pragya Mishra[a], Ashok G. Shende[a], Jagannath[c], Suresh S. Umare[a,*], Rajamma Sasikala[d,*]

[a] Materials and Catalysis Laboratory, Department of Chemistry, Visvesvaraya National Institute of Technology (VNIT), Nagpur, India
[b] CSIR-National Environmental Engineering Research Institute, Nagpur, India
[c] Technical Physics Division, Bhabha Atomic Research Centre Trombay, Mumbai, India
[d] Chemistry Division, Bhabha Atomic Research Centre Trombay, Mumbai, India

ARTICLE INFO

Keywords:
Silver
Silver oxide
Carbon nitride
Microspheres
Degradation

ABSTRACT

Solar light induced photocatalytic oxidative degradation of organic pollutants and bacterial inactivation is an attractive strategy for water purification. Current work is on the use of silver/silver (II) oxide (Ag/AgO) grown *insitu* on the surface of graphitic carbon nitride (g-C_3N_4) as photocatalyst for the effective utilization of solar radiation, as this system can have extended visible light absorption due to the surface plasmon resonance (SPR) phenomenon of metallic silver. Ag/AgO loaded g-C_3N_4 microspheres (Ag/AgO/g-CNMS) were prepared by a facile thermal heating method. The structural and morphological analysis confirmed the existence of metallic Ag and AgO in mixed phase on the surface of carbon nitride. This composite exhibits significant visible light absorption and a reduction in the bandgap compared to g-C_3N_4 due to the SPR exhibited by the metallic silver and lower bandgap of AgO. Photoelectrochemical studies suggest lower charge transfer resistance and better capacitive behaviour for the composite compared to g-C_3N_4. The composite catalyst shows improved photocatalytic performance for the degradation of acid violet-7 dye (AV-7). Besides, it is found to possess significant bactericidal property for the destruction of *Escherichia coli*(*E. coli*) bacteria. This is the first report on the enhanced photocatalytic activity of a silver-g-C_3N_4 system comprising of silver (II) oxide. The present system containing silver (II) oxide shows significantly improved photocatalytic activity and stability compared to the Ag/Ag_2O/g-C_3N_4 with silver (I) oxide reported earlier. The improved performance of the composite is attributed to the increased optical absorption properties and better separation of photogenerated charge carriers. The reactive oxidative species responsible for the degradation reaction is identified and a plausible degradation pathway for the AV-7 dye is presented. Furthermore, this catalyst is found to be stable and does not show any decrease in the photocatalytic activity even after several repeated cycles.

1. Introduction

The emerging environmental contaminants and energy crisis are global issues of concern [1]. Increased urbanization and high living standards burden the environmental health. Immediate addressing of these challenges requires efficient and low-cost techniques. Photocatalytic degradation of organic pollutants by a clean sustainable solar energy based systems is a very promising and attractive strategy. Semiconductor mediated photocatalysis is widely studied for energy and environmental applications. Recently, there is a growing interest for low cost two dimensional g-C_3N_4 based materials. Due to its unique structure, excellent properties as semiconductor and nitrogen richness, make it suitable to act as a metal-free catalyst for a broad variety of photocatalytic applications [2]. However, the photocatalytic performance of bulk g-C_3N_4 is still limited due to its fast recombination of photogenerated electron-hole pairs and moderate visible light absorption capacity ($\lambda < 460$ nm).

To improve the photocatalytic performance of g-C_3N_4, visible light absorption is to be enhanced and efficient separation of charge carriers should occur. Modification of bandgap of g-C_3N_4 through elemental doping or copolymerization has proved to be a successful technique to exploit the structural modifications of g-C_3N_4 [3–5]. Another effective

* Corresponding authors.
E-mail addresses: ssumare@chm.vnit.ac.in (S.S. Umare), sasikala@barc.gov.in (R. Sasikala).

http://dx.doi.org/10.1016/j.apcatb.2017.09.030
Received 24 May 2017; Received in revised form 24 August 2017; Accepted 12 September 2017
Available online 14 September 2017
0926-3373/

way to enhance the photocatalytic performance of g-C_3N_4 is by the construction of semiconductor-semiconductor heterojunctions to promote the charge separation of photo inducted electrons and holes. 2D polymeric g-C_3N_4 with its flexible nature, favors the formation of heterojunctions with various other semiconductors like metal oxides [6–8], mixed oxides [9,10], metal chalcogenides[11,12] and organic semiconductors [13]. Combining g-C_3N_4 with metal atoms such as silver (Ag) facilitate the migration and separation of charge carriers with easy mass diffusion [14]. Reports of g-C_3N_4/silver based heterojunctions are available, where g-C_3N_4 is combined with Ag_2O [15], Ag_2CO_3 [16], Ag_3PO_4 [17,18], Ag_3VO_4 [19], Ag_2S [20], AgCl [21], AgBr [22], and AgI [23], all of which enhance the photocatalytic performance of bulk g-C_3N_4.

In our current work, we report the use of Ag/AgO/g-C_3N_4 microspheres (Ag/AgO/g-CNMS), for the photocatalytic degradation of AV-7 dye and effective antimicrobial activity under visible light irradiation. It is known that the optical properties and bandgap of silver oxide varies with the synthesis methods from 1.12-1.71 eV [24–26]. Hence, silver oxide was synthesized by an *in situ* growth of Ag/AgO on g-C_3N_4 in which 2D g-C_3N_4 sheets were moulded to 3D spheres using SiO_2 hard template. In this system, a co-existence of bivalent silver (II) oxide with metallic Ag^0 is observed on g-C_3N_4 to form a novel combination of photocatalyst. Although, several studies on Ag/Ag_2O/g-C_3N_4 are already reported, where Ag exists in +1 oxidation state, to the best of our knowledge, a combination of g-C_3N_4 and Ag/AgO has never been addressed. It is expected that Ag/AgO with g-C_3N_4 can improve the visible light absorption and enhance the separation of photogenerated charge carriers, which can increase its photocatalytic efficiency.

2. Experimental section

2.1. Materials

All the chemicals, melamine (Finar Chem. Ltd, 99%), silver nitrate ($AgNO_3$) GR grade (Merck, India), tetraethyl orthosilicate (TEOS) (Aldrich, 98%), Acid Violet-7 (Aldrich, dye content ca. 85%), were of analytical grade and used without any further purification. Millipore water (conductivity < 0.15 mS cm^{-1}) was used throughout the experiments.

2.2. Synthesis of Ag/AgO/g-CNMS

10 g of melamine was dissolved in 100 mL of millipore water and 5 mL of 4 M HCl. To this 6 mL of TEOS was added instantly and stirred for 5 min. This was followed by the addition of calculated amount of $AgNO_3$ and liq·NH_4OH (5 mL). The obtained product was washed with acetone and dried at 80 °C for 2 h. The white powder obtained was annealed at 550 °C for 2 h in a muffle furnace to obtain a pale grey colored compound. This powder was treated with $NH_4.HF_2$ and kept it overnight to remove SiO_2 and to obtain Ag/AgO/g-CNMS grey powder. Concentration of $AgNO_3$ was varied to synthesize different Ag/AgO(x)/g-CNMS composites where x = 1, 2, 5, 10, 15 and 20% by weight.

2.3. Characterization

XRD analysis of the samples was performed for the structural characterization in the 2 θ range between 10° and 80° using an X-ray diffractometer (Rigaku: Miniflex-II-DD34863) using Cu Kα radiation (λ = 0.15418 nm) operated at 30 kV and 15 mA at a scan rate of 5° min^{-1}. X-ray photoelectron spectroscopy (XPS) studies were carried out on a VG Microtech electron spectrometer using Mg Kα X-rays (hν = 1253.6 eV) as the primary source of radiation. The chamber pressure was maintained at 1×10^{-9} Torr. Appropriate correction for charging effect was made with the help of the C 1 s signal appearing at 284.5 eV. XPS Peak 4.1 software was used to fit the XPS peaks. The decomposition of the spectra curves into individual components was performed using a combination of Gaussian and Lorentzian functions after background subtraction by the Shirley method. The TEM images were taken using a FEI Tecnai T-20 electron microscope operating at 300 kV. Energy dispersive X-ray spectroscopy analysis was carried out using Zeiss FESEM. UV–vis diffuse reflectance spectra (UV–vis DRS) of all samples were recorded using a Jasco (model V-670) spectrophotometer equipped with an integrating sphere accessory. Barium sulfate was used as reference for the reflectance spectra. Electrochemical studies were carried out by a PARSTAT 4000 (Princeton Applied Research, Ametek, USA) Potentiostat/Galvanostat using a conventional three-electrode system. Thermogravimetric analysis of prepared catalyst was carried by using a thermal analyzer TG-DTA 7200 (Hitachi). The identification of degradation products was performed by using a Waters Micromass Q-TOF mass spectrometer, Waters Alliance 2795 electrospray ionization mass spectrometry (ESI–MS). Inductively Coupled Plasma–Mass Spectrometer (Perkin Elmer, NexION 300x) used for tracing of Ag metal leaching.

2.4. Photocatalytic experiments

The photocatalytic activity of the prepared Ag/AgO/g-CNMS was evaluated for the degradation of 20 mgL^{-1} aqueous solution of Acid Violet-7 (AV-7) dye. Degradation experiments were performed in a lab made photo-irradiator fitted with compact fluorescent lamps (12 lamps of 100 W each, Oreva) vertically and equidistantly on the base of the rectangular galvanized iron chamber containing air circulation to minimize the heating effect. The radiation of these lamps mainly contains visible light along with very low amount of UV light (~3%). For each photocatalytic experiment, 100 mL of aqueous AV-7 (20 mgL^{-1}) solution was taken in a beaker containing 0.1 g of catalyst under ambient conditions. Prior to irradiation, reaction mixture was magnetically stirred in the dark for 30 min to ensure uniform dispersion and adsorption-desorption equilibrium between the dye molecules and the catalyst surface. The photocatalytic activity was measured by taking a small volume of clear supernatant liquid from reaction mixture at regular intervals of time, centrifuged it and analyzed by UV–vis Spectrophotometer (Shimadzu, UV-1800) at λ_{max} = 523 nm. Concentration of solution remained unchanged when it was irradiated without catalyst and in dark control experiment.

2.5. Bacterial culture and antimicrobial test

Autoclave sterilized glassware were used for antibacterial test experiments. Gram-negative *Escherichia coli* (*E. coli*) (ATCC 25933) were used as a target microorganism for antimicrobial tests. For photocatalytic antimicrobial experiments, *E. coli* was transferred to 30 mL of liquid Luria Bertani (LB) culture medium from solid LB agar plate and grown at 28 °C for 12 h. Then the bacteria were diluted with broth to 10^5 cfu/ml and concentration of bacteria was determined by measuring optical density at 600 nm. Calculated amount of catalyst was suspended in 30 mL of *E. coli* culture medium and illuminated under visible light source. The light source of illumination used was 100 W tungsten lamp located at 22 cm away from the sample. To quantify the antimicrobial test, about 1 mL of the catalyst suspended bacterial mixture was withdrawn after the photo irradiation. To ensure the growing bacterial colonies were legible, 0.1 mL of the treated solution was spread on solid LB medium and continued to incubate at constant temperature of 28 °C for 24 h, and then counted to determine the bactericidal efficiency. For better comparison, control experiments were carried out simultaneously without catalyst and without light illumination. The amount of catalyst used for antimicrobial study was optimized. The percentage of growth inhibition was determined by comparing the survival colony counts with corresponding colony counts of control sample.

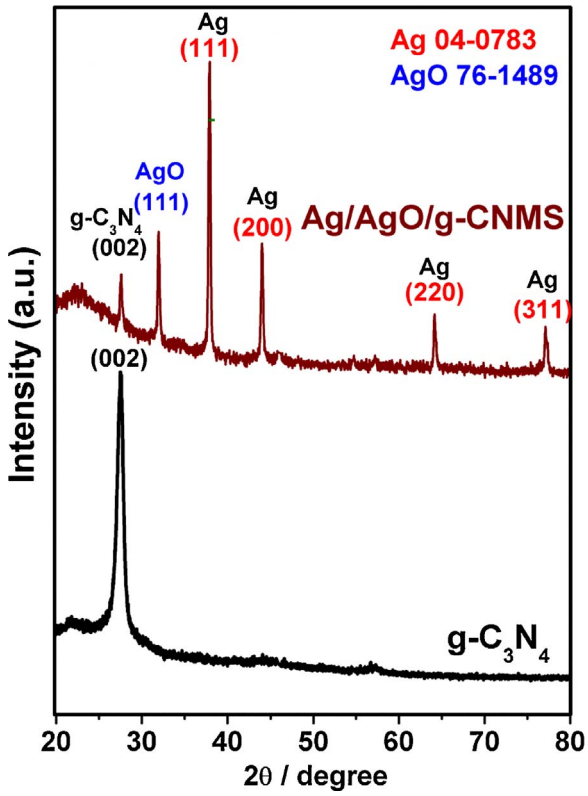

Fig. 1. Powder X-ray diffraction patterns of gC_3N_4 and Ag/AgO/g-C_3N_4 microspheres.

2.6. Photoelectrochemical study

The electrochemical characterization of Ag/AgO/g-CNMS composite was measured by coating as prepared materials on stainless steel (SS) substrate (1 cm X 5 cm, 305 grades). The cyclic voltammetry (CV) analysis performed by immersing coated SS electrode in saturated aqueous solution of 1 M KOH.

3. Results and discussion

Phase identification and composition of Ag/AgO/g-CNMS samples were performed by powder X-ray diffraction analysis (XRD). XRD pattern of Ag/AgO(10%)/g-CNMS heterostructure (Fig. 1) showed distinctive peak of g-C_3N_4 at $2\theta = 27.5^{\circ}$ corresponding to aromatic interlayer-stacking (002) reflection [27]. Besides, peaks at $2\theta = 37.9^{\circ}$, 44.1° and 64.2° are seen, which are attributed to the reflections from (111), (200) and (220) planes respectively of cubic $Fm\bar{3}m$ space group of metallic silver (JCPDS file no.87-0597). The peak at $2\theta = 31.9^{\circ}$ may correspond to (111) plane of cubic AgO (JCPDS file no.76-1489) [28]. These results suggest the coexistence of both Ag and AgO phases in the formed samples. The formation of cubic structured AgO (II) is very rarely reported, and existence of Ag^{+2} in prepared Ag/AgO/g-CNMS composite is further evidenced by high resolution Ag 3d XPS analysis.

The morphology, particle size and shape of the as synthesized Ag/AgO/g-CNMS samples were investigated using scanning electron microscopy (SEM) and transmission electron microscopy (TEM). SEM image of Ag/AgO(10%)/g-CNMS exhibits well dispersed microsphere like structures (Fig. 2 **and Fig. S1**). The size of microspheres vary between 3 and 15 μm and the elemental mapping of representative Ag/AgO(10%)/g-CNMS confirms the dispersion of C, N, O and Ag all over the microsphere structure (Fig. 2). The typical TEM image of Ag/AgO (10%)/g-CNMS exhibits Ag capped AgO sphere like structures on the surface of carbon nitride (Fig. 3**a**). SAED pattern exhibits few bright diffraction spots confirming the existence of crystalline Ag capped on AgO (Fig. 3**b**). HRTEM image shows lattice fringes with interplanar 'd' spacings of ca. 0.27 and 0.20 nm corresponding to (111) crystal plane of AgO and (200) plane of Ag respectively (Fig. 3**c**). These results support the formation of Ag/AgO/g-CNMS.

The Ag/AgO functionalised g-C_3N_4 was investigated by Fourier transform infrared spectroscopy (FT-IR) analysis (Fig. 4). The stretching frequency at ca. 3290 cm^{-1} (broad) is ascribed to the N—H stretching vibration modes of $-NH_2$ or =NH groups as uncondensed amine groups of g-C_3N_4 [29,30]. The absorption bands in the region of 1700-1200 cm^{-1} can be ascribed to the vibrations of C—N heterocycles [31–33]. The band at 809 cm^{-1} (sharp) corresponds to the breathing mode of triazine groups in g-C_3N_4 [15], the spectrum of Ag/AgO/g-CNMS shows a broadening of all bands compared to g-C_3N_4. The intensity of the band present at 809 cm^{-1} has decreased due to the presence of Ag/AgO on the surface of g-C_3N_4 and this observation is in conformity with the FT-IR results of Ag_2O/g-C_3N_4 reported earlier [15].

Further, the chemical composition and oxidation states of silver in Ag/AgO(2%)/g-CNMS composite were characterized by X-ray photoelectron spectroscopy (XPS). The high-resolution Ag 3d XPS of Ag/AgO/g-CNMS spectrum is fitted as two doublets (Fig. 5**a**). The peak positions of $3d_{5/2}$ and $3d_{3/2}$ corresponding to one of the doublets are 367.4 and 373.4 eV respectively. The binding energy (BE) values for the other doublet are 368.2 and 374.1 eV. Previous reports suggest that the peaks in the BE range 368.1–367.9 and 374.1–373.9 eV corresponds to metallic silver [34]. Hence, the peaks seen at 368.2 and 374.1 eV can be assigned to the metallic silver present in the composite sample. The peaks seen at BE of 367.4 and 373.4 eV are attributed to the Ag^{2+} state [34,35]. The negative BE shift of Ag^{2+} from metallic silver is discussed in detail by Weaver et al. [35] and has been attributed to the difference in the electro negativity values of Ag metal and its cation. Thus, the result of XPS is in conformity with the obtained XRD results showing the existence of both Ag metal and Ag(II)O. The N1 s spectra of g-C_3N_4 and Ag/AgO/g-CNMS are shown in (Fig. 5**b**). The spectra are broad having a clear asymmetry towards higher binding region. The spectrum of g-C_3N_4 was fitted as two peaks at BE values of 398.2 and 400.0 eV, which can be assigned to the sp^2 bonded N atoms in the triazine ring and to the bridging N atoms in the $N-(C)_3$ group respectively [36,37]. The spectrum of the composite also shows similar peaks, whose BE values are close to that of N1 s of g-C_3N_4. The C 1 s spectra of g-C_3N_4 and the composite are shown in (Fig. 5**c**). The spectrum of g-C_3N_4 is fitted as three peaks having BE values of 284.5, 286.4 and 288.1 eV. The peak at 284.5 is due to the presence of adventitious carbon and the latter two are attributed to the chemical bond between C and N atoms in g-C_3N_4 [37,38]. All these three peaks are seen in Ag/AgO/CNMS sample except that the intensity of the adventitious carbon is more in the composite compared to g-C_3N_4. This can be due to the surface coating of g-C_3N_4 by Ag-AgO. The O 1 s spectrum obtained from Ag/AgO(2%)/g-CNMS has predominant O feature due to AgO with B.E of 529.0 eV and it is assigned to lattice oxygen atom of silver oxide (Fig. 5**d**) [33]. The second peak present at 530.2 eV can be assigned to the small amount of carbonates present on the surface [39,40]. The surface concentration of Ag^0 and Ag^{2+} was estimated from the XPS peak area and the values are found to be 2.5 and 2.4 Atom% respectively.

UV–vis absorption spectra of g-C_3N_4 and Ag/AgO(10%)/g-CNMS are shown in (Fig. 6). The UV–vis spectrum of Ag/AgO(10%)/g-CNMS shows significantly improved visible light absorption compared to bulk g-C_3N_4 (Fig. 6**a**). The enhanced visible light absorption can be attributed to a combined effect of surface plasmon resonance (SPR) of metallic silver and a lower bandgap of AgO [41–43]. Band gap of g-C_3N_4 and Ag/AgO(10%)/g-CNMS has been calculated from the transformed Kubelka-Munk (KM) plots of $(F_{(R)}h\nu)^2$ *vs.* photon energy (Fig. 6**b**). The bandgap values of g-C_3N_4 and the composite are 2.76 and 2.48 eV respectively. Thus, the composite microsphere has a narrow band gap compared to g-C_3N_4, which can extend the optical absorption to longer wavelengths.

The interfacial charge transfer properties in this composite were

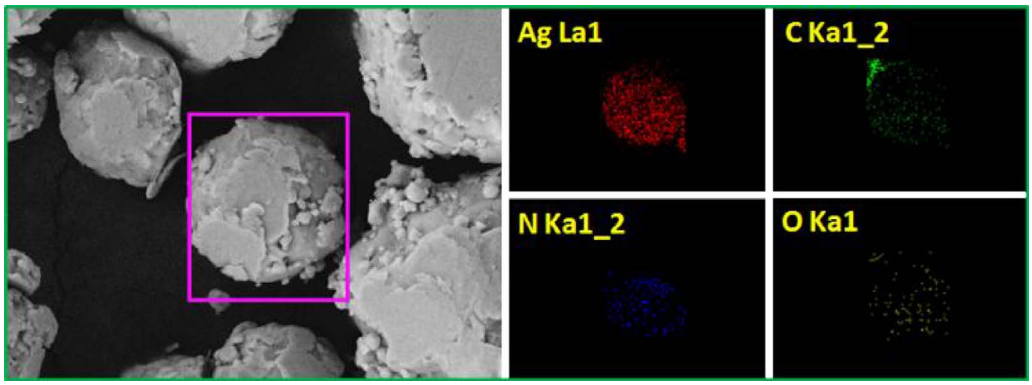

Fig. 2. Selected portion of Ag/AgO/g-CNMS-10 composite SEM image with elemental mapping.

studied by electrochemical impedance spectroscopy (EIS). The Nyquist plot of Ag/AgO(10%)/g-CNMS and g-C_3N_4 under ambient conditions is presented in (Fig. 7**a**). The semicircle of the curve represents the charge transfer resistance. [44] A smaller semicircular arc of Ag/AgO(10%)/g-CNMS compared to g-C_3N_4 indicates that the composite sample has lower charge transfer resistance. Hence, separation of charge carriers can be better in the composite than that in g-C_3N_4. The cyclic voltammogram (CV) curves of g-C_3N_4 and Ag/AgO(10%)/g-CNMS at a potential range from −1 to +0.1 V (vs. Ag/AgCl) and at a scan rate of 50 mV S^{-1} is shown in (Fig. 7**b**). CV voltammogram of Ag/AgO(10%)/g-CNMS displayed a large capacitive area and better electrochemical performance than pristine g-C_3N_4. This might be due to the presence of silver oxide on the g-C_3N_4 skeleton [45]. Loading of Ag/AgO enhances the conductivity and facilitates easy electronic transmission from triazine structure of g-C_3N_4 to AgO/Ag. This characteristic ideal capacitive behavior of Ag/AgO(10%)/g-CNMS is in conformity with the results of electrochemical impedance spectroscopy studies (EIS). The galvanostatic charge-discharge (GCD) curves for these samples are shown in (Fig. 7**c**). The GCD profile for a fixed current density of 1.5 Ag^{-1} of g-C_3N_4 shows a fast charging and discharging behavior whereas in the case of Ag/AgO/g-CNMS the charge-discharge time is a little longer. These results indicate the supercapacitance properties of composite samples.

Thermal stability of Ag/AgO(10%)/g-CNMS is examined by performing thermogravimetric (TG) analysis under inert atmosphere of N_2. The thermogram of Ag/AgO(10%)/g-CNMS shows two distinct weight loss temperatures at 426 °C and 483 °C **(Fig. S2)**. About ca. 2% of weight loss in the range of 120–180 °C is due to physically adsorbed water. While a steep ca. ~5% weight loss in between 420 and 480 °C is may be due to the thermal decomposition of AgO to Ag_2O with loss of oxygen [24]. Further heating above 600 °C causes complete decomposition of carbon nitride frame work into graphite and N_2 [46]. DTG thermogram has two distinct sharp endothermic peaks at 452 °C and 564 °C corresponding to decomposition of metal oxide. TG analysis

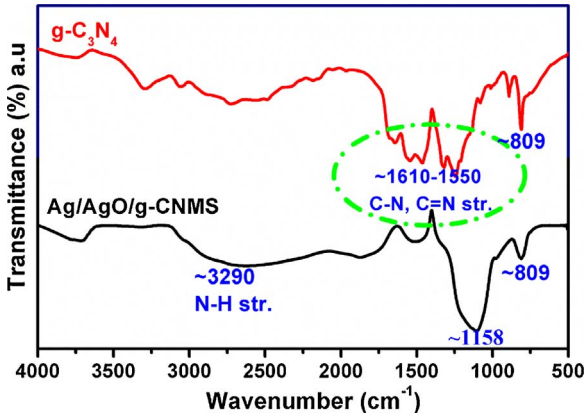

Fig. 4. FTIR spectra of g-C_3N_4 and Ag/AgO/g-CNMS photocatalyst.

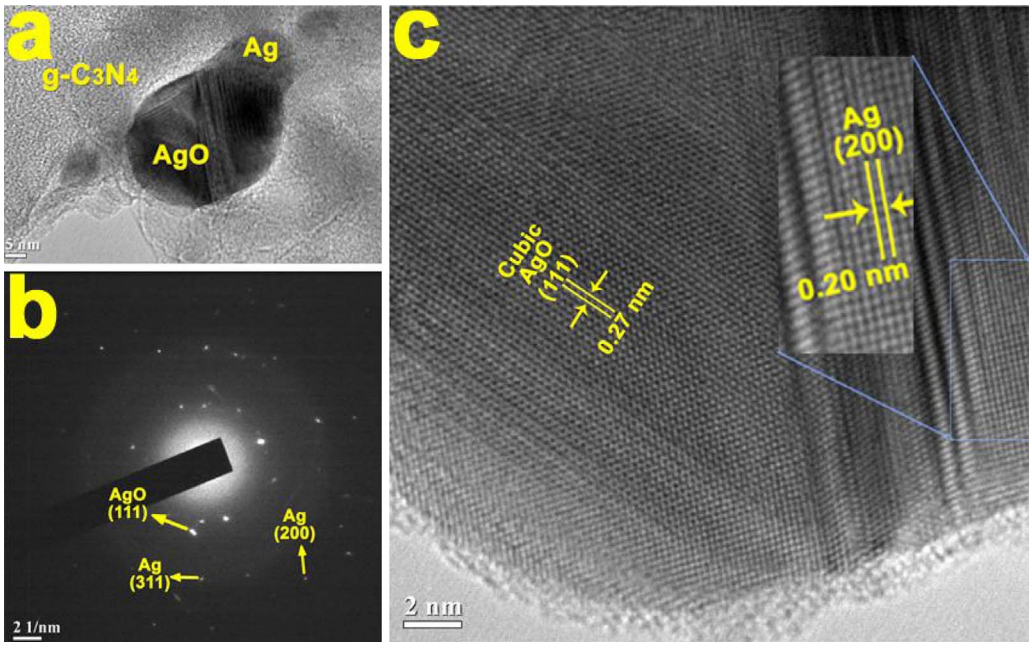

Fig. 3. (a) TEM image (b) HRTEM and (c) SAED pattern of Ag/AgO/g-CNMS.

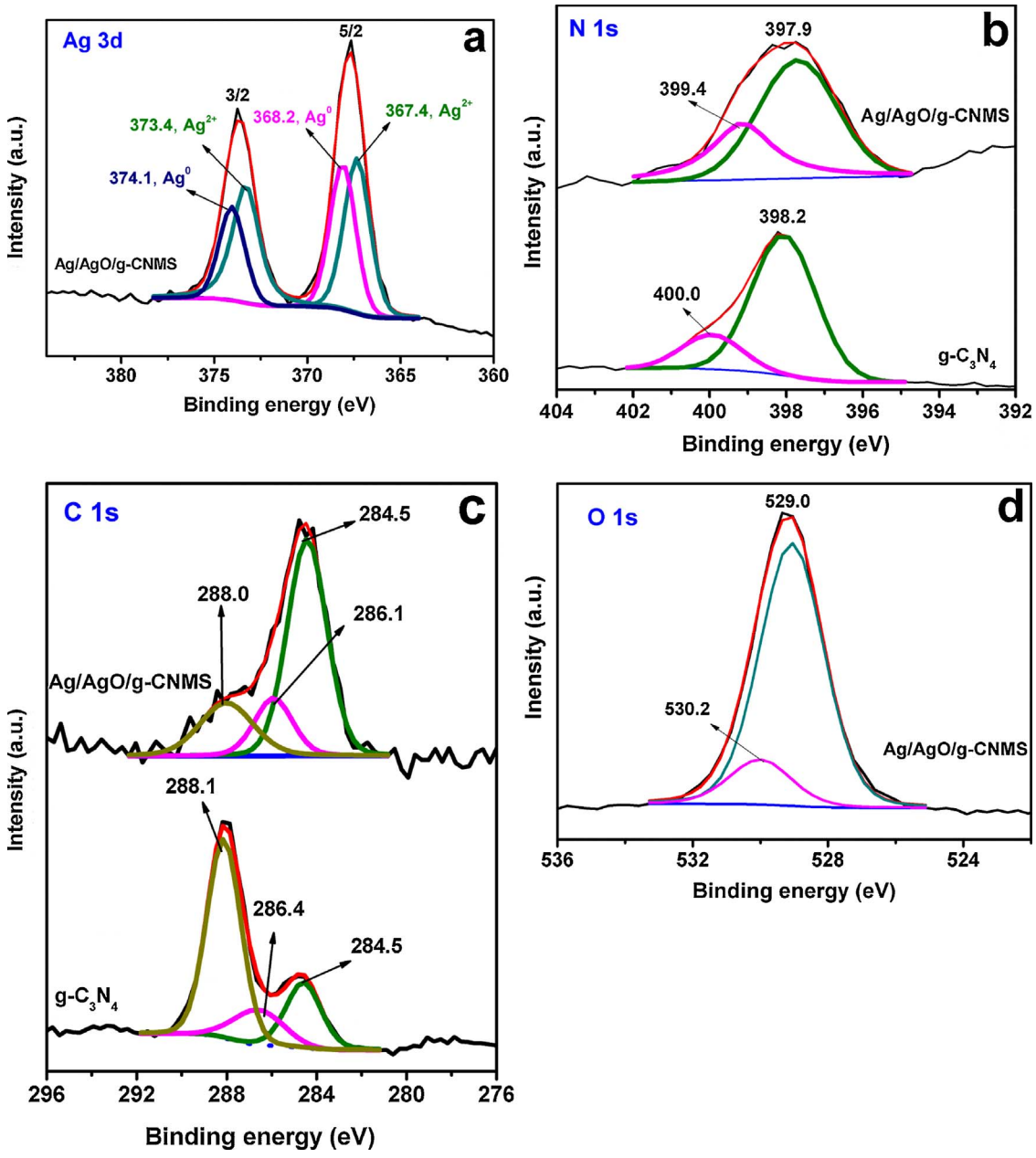

Fig. 5. XPS profiles of (a) Ag 3d (b) N 1 s (c) C 1 s and (d) O 1 s spectra of Ag/AgO/g-CNMS.

suggests that the composite sample is stable up to 400 °C.

3.1. Photocatalytic dye degradation

The effect of Ag/AgO weight% loading onto the g-C_3N_4 microspheres to degrade 20 mg L^{-1} AV-7 dye was studied (Fig. 8). It has been found that increase in loading of Ag/AgO wt% increases the degradation process up to 10 wt%. Further, increase in Ag loading resulted in the reduction of reaction rate which is attributed to the deactivation of g-C_3N_4 surface active sites due to the aggregation of Ag particles and low absorption of light. The amount of catalyst dose required to get the highest efficiency to degrade 20 mg L^{-1} of AV-7 dye was studied by varying amount of catalyst between 0.15–0.40 g. Increasing the amount of catalyst from 0.10 to 0.30 g in 100 mL of aqueous AV-7 dye results in an increase in the degradation efficiency from 78% to 98% after 10 min of reaction time **(Fig. S3)**. Further increase in the amount of catalyst results in a decrease of the degradation efficiency. Thus, further experiments were performed with this optimum amount of catalyst.

In order to study the effect of pH on rate of degradation, degradation experiments were performed under varied pH, ranging from 3.0 to 9.0 pH by addition of either 0.1 M HCl or NaOH **(Fig. S4)**. Acidic conditions of the reactions have shown greater reaction rate than in basic pH, which is known to occur for anionic dyes [47]. Stability and recyclability of the composite catalyst was evaluated by performing repeated degradation cycles. After each cycle the photocatalyst was recovered by centrifugation followed by washing with acetone and drying in an oven in air for 2 h at 120 °C. The photocatalyst shows negligible decrease in the degradation efficiency after four repeated cycles **(Fig. S5)**. XRD of catalyst after four repeated cycles is similar to the fresh sample indicating Ag/AgO(10%)/g-CNMS photocatalyst is stable and reusable **(Fig. S6)**. In order to further check the stability of this catalyst and the possibility of Ag^+ ions leaching out at different pH conditions, experiments were performed by dispersing the catalyst in varied pH solutions and the eluents were analyzed by inductive coupled plasma mass spectroscopy (ICP-MS), which could not detect any silver ions. This rules out the possibility of Ag^+ leaching under different

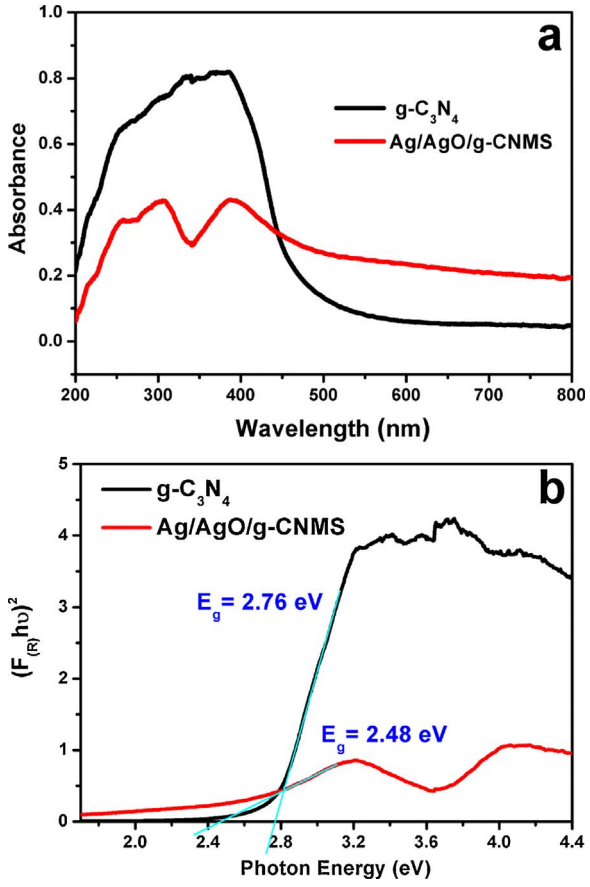

Fig. 6. Comparative (a) UV–vis absorption spectra and (b) Kubelka-Munk plots of g-C_3N_4 and Ag/AgO/g-CNMS.

experimental conditions, which confirms the stability of the material.

3.2. Reaction mechanism and degradation pathway

The conduction band (CB) and valence band (VB) potentials of g-C_3N_4 are −1.12 and +1.57 V respectively. The relative CB and VB potentials of AgO were calculated using the equations.

$$E_{(CB)} = \chi\text{-}E_c\text{-}0.5\ E_g$$

$$E_{(VB)} = E_{(CB)}\text{-}E_g$$

Where 'χ' is the absolute electronegativity of the semiconductor, which is the geometric mean of the absolute electronegativity of the constituent atoms, and expressed as the arithmetic mean of the atomic electron affinity and the first ionization energy; 'E_c' is the energy of free electrons on the hydrogen scale (4.5 eV); and 'E_g' is the band gap energy of a semiconductor. The CB and VB edge potentials obtained are +0.72 and +1.84 V respectively.

To determine the main reactive oxygen species (ROS) responsible for degradation of AV-7, the carrier trapping experiments were performed with radical scavengers **(Fig. S7)**. Photocatalytic degradation experiment was performed using isopropanol (2 mL) to quench hydroxyl radicals (OH·), p-benzoquinone (10^{-3} M, 5 mL) for superoxide ($O_2^{\bullet-}$) and ammonium oxalate (0.1 g) for hole(h^+) quenching. The addition of these scavengers led to a significant decrease in the degradation rate and photocatalytic activity, suggesting that all three species play a significant role in the degradation of AV-7 dye.

The possible reactions occurring during the photocatalytic degradation of AV-7 can be as given below. [48,49]

$$g\text{-}C_3N_4 + h\nu \rightarrow h^+_{(VB)} + e^-_{(CB)} \quad (1)$$

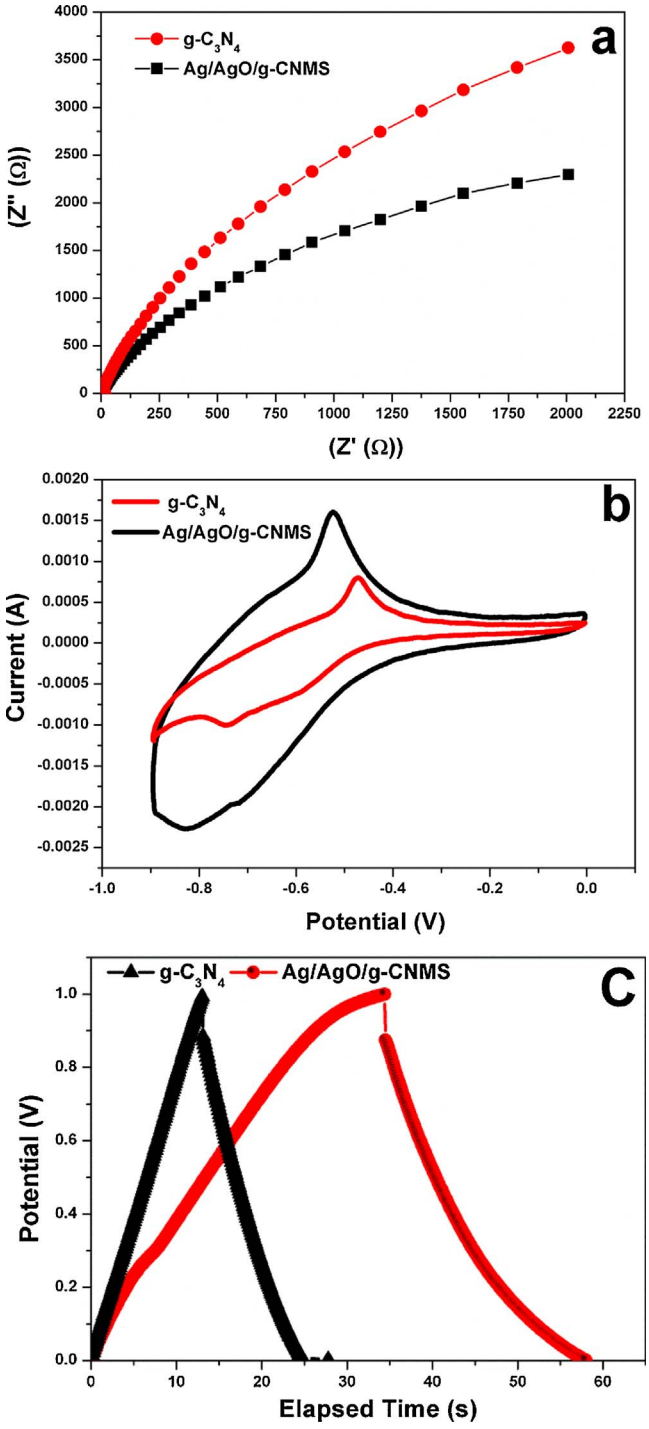

Fig. 7. (a) Nyquist plot (b) CV and (c) galvanic charge discharge plots of gC_3N_4 and Ag/AgO/g-CNMS.

$$AgO + h\nu \rightarrow h^+_{(VB)} + e^-_{(CB)} \quad (2)$$

$$O_2 + e^-_{(CB,g\text{-}C_3N_4)} \rightarrow O_2^{-\bullet} \quad -0.2\ V \quad (3)$$

$$O_2^{-\bullet} + 2H_2O + 2\ e^-_{(CB)} \rightarrow 3OH^- + OH^{\bullet} \quad +0.9\ V \quad (4)$$

$$OH^- + h^+_{(VB)} \rightarrow OH\cdot \quad +1.3\ V \quad (5)$$

$$AV\text{-}7 + OH^{\bullet} \rightarrow \text{degradation products}$$

$$AV\text{-}7 + h^+_{(VB)} \rightarrow \text{degradation products}$$

$$h^+_{(VB)} + H_2O \rightarrow H^+ + OH\cdot \quad +2.8\ V \quad (6)$$

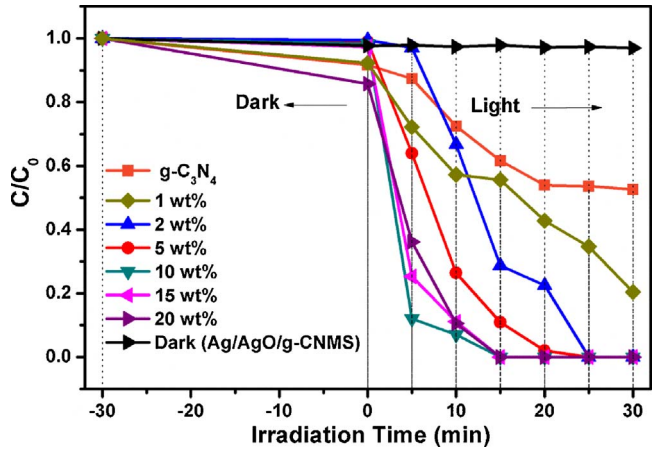

Fig. 8. Effect of Ag (wt%) loading on the degradation of 20 mg L^{-1} AV-7 dye.

In this composite system, AgO cannot initiate the Reactions (3) and (6) as the CB and VB potentials are not suitable for these reactions [50]. It may also be noted that the oxidation potential of the valence band hole of g-C_3N_4 is not sufficiently positive for generating OH· radical from water by the Reaction (6) [48]. However, $OH^{\bullet}$ radicals can still be produced in this system by the reaction as shown in Eqs. (4) and (5). AV-7 dye can be oxidised by the strong oxidising radicals like OH· and photogenerated holes ($h^{+}_{(VB)}$).

To assess the key intermediate products formed during the photodegradation of AV-7, aliquots obtained after five, ten and twenty minutes of light irradiation were investigated by ESI (−)-MS analysis and results are presented in (Fig. S8). Based on the main fragmentation products observed in ESI (−)-MS analysis, a plausible AV-7 degradation pathway is proposed as given in Scheme 1. The initial transformation product of AV-7, observed in ESI (−)-MS spectrum with m/z ratio of 521 is attributed to anionic state of AV-7 dye. The oxidative cleavage and desulfonation of AV-7 anionic form could transform into dihydroxylated naphthalene forms (**1a, 1b**) with m/z ratio of 260. Further hydroxylation of **1a and 1b** led to the formation of several prominent fragments as shown in **2a, 2b, 2c** with m/z ratio of 170, 174 and 179. Finally, repetitive ROS attack results in the formation of lower molecular weight N-phenyl amide and hydrocarbon products (**3a, 3b**) with m/z ratio of 134 and 96, which were further mineralised into CO_2 and H_2O.

The enhanced photocatalytic activity of the composite microspheres compared to g-C_3N_4 is due to the improved optical absorption and better separation of charge carriers. UV–vis spectra and photoelectrochemical studies clearly substantiate these observations. The enhanced capacitive behaviour of the composite can also play a role in increasing the photocatalytic activity [51]. The improved charge storage capacity of the composite is a proof that the separation of charge carriers is occurring in the composite more effectively, resulting in a significant improvement in its photocatalytic activity. The presence of excess charge carriers on catalyst surface can induce the formation of reactive oxidative species, which are essential for degradation of organic pollutants [51].

Besides, Ag metal by virtue of its SPR phenomenon can generate O_2^{-} ions which facilitate the oxidation of the dye molecules [52]. The

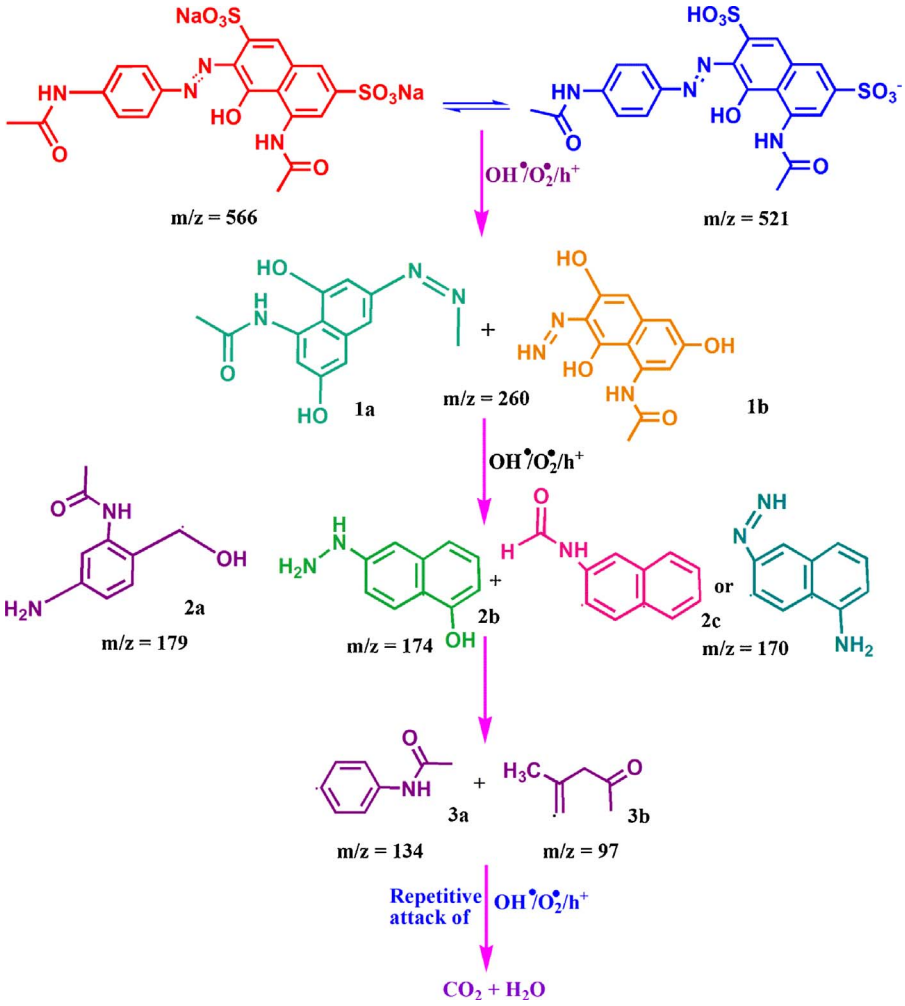

Scheme 1. Plausible degradation pathway of AV-7 using Ag/AgO/g-CNMS photocatalyst.

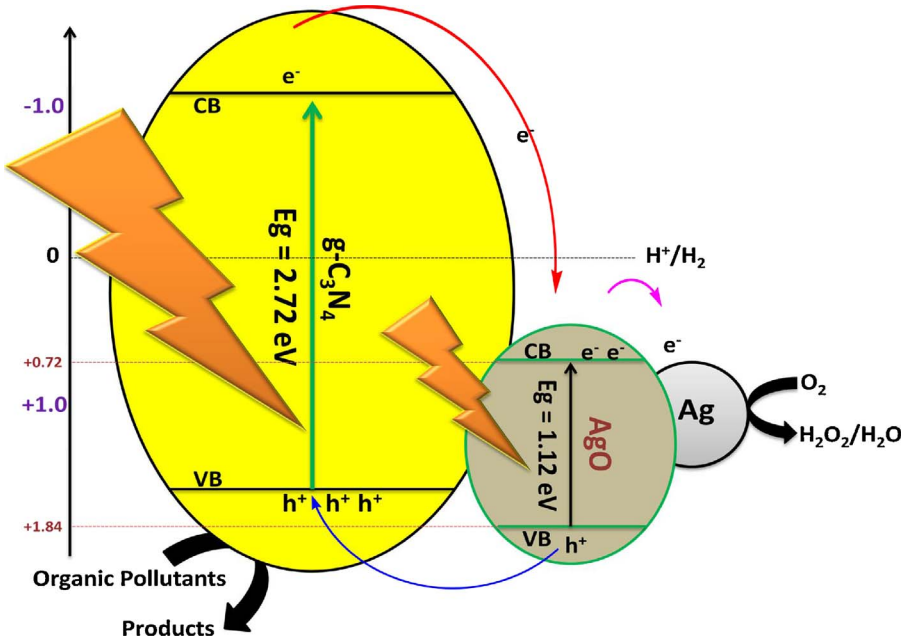

Fig. 9. Schematic illustration of electron transfer in Ag/AgO/g-CNMS composite.

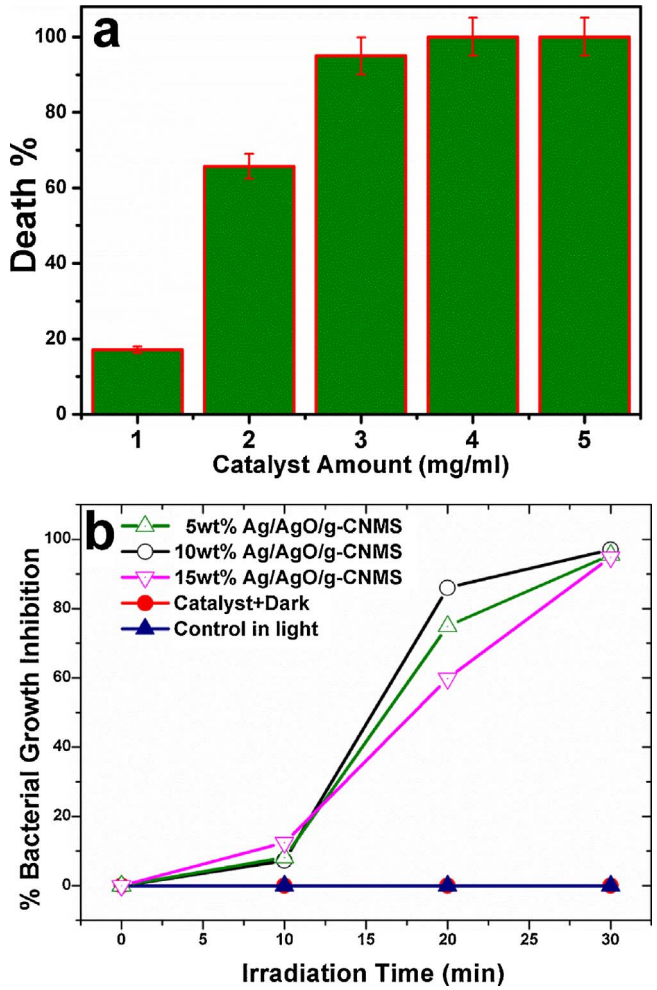

Fig. 10. (a) Effect of catalyst amount on growth inhibition of *E. coli* bacteria (b) *E. coli* growth inhibition rate over Ag/AgO/g-C_3N_4 photocatalyst.

energy required to transfer an electron to the antibonding orbital of O_2 adsorbed on Ag is 2.4 eV and this energy is the same as the surface plasmons of Ag. Another factor for the improved activity of the composite is that, AgO due to its lower band gap can extend the optical absorption to longer wavelengths, which increases the photocatalytic activity. The lower charge transfer resistance of the composite microspheres compared to g-C_3N_4, indicated by the impedance studies, shows the ease of charge transfer process in the composite, which in turn minimises the electron-hole recombination. A schematic of the charge separation process which can occur in this composite system is shown in (Fig. 9). As the CB potential of AgO is at a lower level than that of g-C_3N_4, the photogenerated electron can get transferred to the CB of AgO and from there it can further get transferred to Ag metal. As the VB potential of AgO is more positive than g-C_3N_4, the photogenerated holes can migrate to g-C_3N_4 and hence the charge carriers can get separated well in the composite system. All these factors lead to enhanced photocatalytic activity.

A comparison of the photocatalytic performance of earlier reported silver/silver (I) oxide g-C_3N_4 with the present Ag/Ag(II)O/g-CNMS system is made and the same is summarised in **Table S1**. The data clearly show that the Ag/Ag(II)O/g-CNMS system of this study is highly efficient and has better photocatalytic activity than the existing Ag/gC_3N_4 or Ag/Ag(I)O/g-C_3N_4. Other systems like Ag_2O/g-C_3N_4 also show comparatively lower efficiency compared to the present Ag (II) system [53]. The excellent thermal stability and reusability of Ag/Ag(II)O/g-CNMS photocatalyst, as described in TG and recyclability analysis is another important property of this system. Besides, Ag/Ag(II)O/g-CNMS was found to be efficient for solar disinfection of bacterial pathogens. The details of these experiments are given in the following section.

3.3. Antimicrobial activity

Antibacterial performance of Ag/AgO(10%)/g-CNMS was evaluated against the growth of a gram-negative *Escherichia coli* (*E. coli*) culture. To find optimum amount of catalyst required for complete growth inhibition of *E. coli*, experiments were performed using 1, 2, 3, 4, and 5 mg/mL of the catalyst. There was low quantitative growth inhibition when 1 mg and 2 mg of catalyst was used amounting to ca. 17% and 65% growth inhibition respectively. However, use of 3 and 4 mg of catalyst inhibited ca. 97% and 99% growth of *E. coli* respectively. Thus,

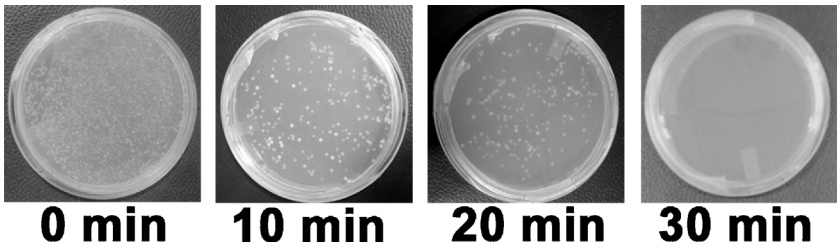

Fig. 11. Survived culture growth of *E. coli* incubated with Ag/AgO/g-CNMS under visible light irradiation, samples drawn at fixed time intervals of 0–30 min. Images are taken after incubation on LB medium for 24 h.

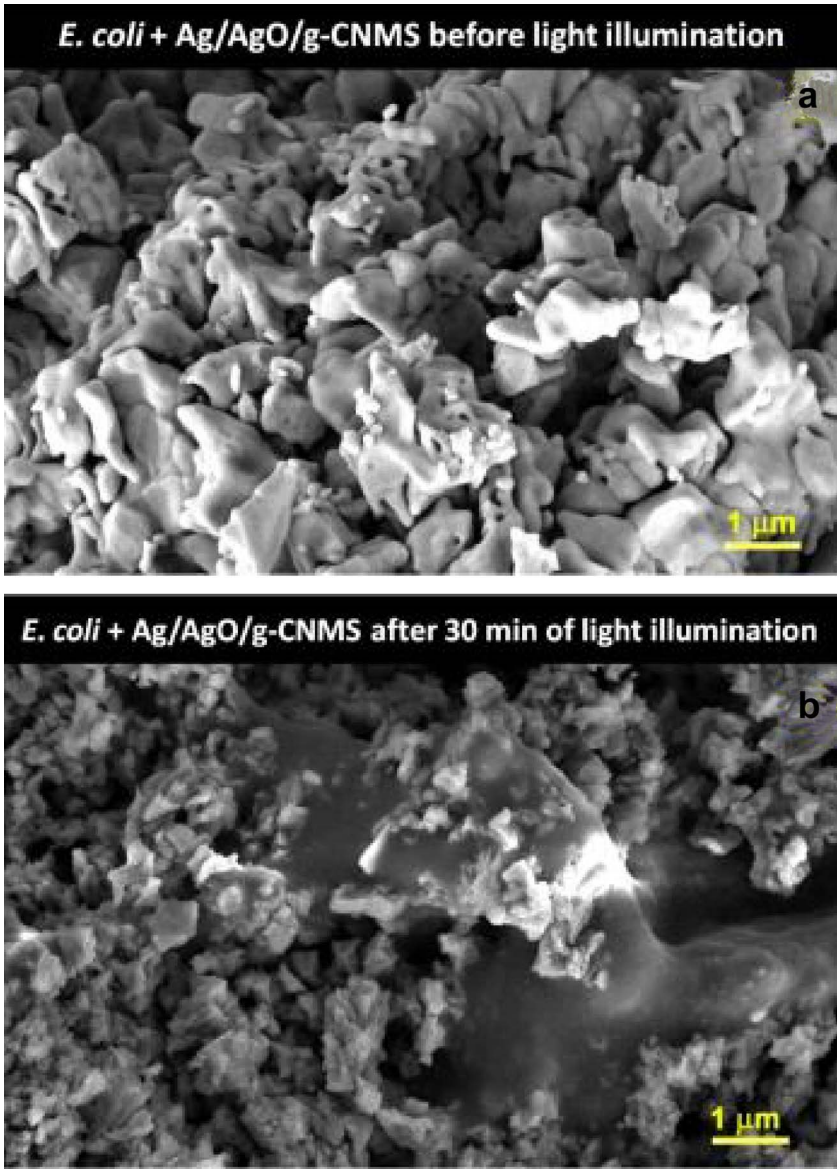

Fig. 12. SEM images of E. coli suspended with Ag-AgO/g-CNMS catalyst (a) before and (b) after visible light illumination.

optimum amount of catalyst for almost complete destruction of *E. coli* is 5 mg and further studies have been carried out with this optimized amount of catalyst (Fig. 10**a**).

The optimum concentration of Ag/AgO required on g-C_3N_4 to get the best disinfection efficiency was investigated by varying the amount of Ag/AgO on g-C_3N_4. It can be seen from Fig. 10**b** that the growth inhibition is faster when 10%Ag/AgO/g-CNMS is used. After 20 min of exposure to light, the growth inhibition induced by 5%, 10% and 15% Ag/AgO on g-C_3N_4 are 74, 86 and 59% respectively. This suggests that for the *E. coli* disinfection process also, the optimum concentration is 10%Ag/AgO on g-C_3N_4 (Fig. 10**b**). Further, control experiment confirms the low or no toxicity of the catalyst on *E. coli* bacterial cell. *E. coli* suspended with Ag/AgO(10%)/g-CNMS photocatalyst has regular growth under dark conditions even after 45 min, signifying the photocatalytic growth inhibition of microorganism.

Optical images were taken to check the growth density of *E. coli* colonies after 10, 20 and 30 min of light irradiation (Fig. 11). Acute destruction of *E. coli* cells was observed within 30 min of light exposure. These results also support the photo-bactericidal performance of Ag/AgO(10%)/g-CNMS photocatalyst on *E. coli* cells under visible light irradiation. SEM images were taken to illustrate the effect of Ag/AgO (10%)/g-CNMS coating on the morphology of *E. coli cells*. SEM images of *E. coli* suspended with photocatalyst, without exposure to light exhibit special nodule-like morphology along with certain well dispersed

rod shaped *E. coli* cells. SEM images taken after photo irradiation exhibit damaged cell morphology. Further, no rod shaped survived bacterial cells are observed (Fig. 12). These SEM results confirm the effective visible-light induced inactivation of *E. coli* cells over Ag/AgO (10%)/g-CNMS photocatalyst.

To understand the mechanism of disinfection, isopropanol and sodium oxalate were used as scavengers for OH· and VB h^+. The bacterial inactivation of *E. coli* was greatly reduced in the presence of isopropanol and sodium oxalate quenchers. The use of sodium oxalate has substantially increased the growth of survived bacterial colonies **(Fig. S9)**. This result implies that VB h^+ and OH are major reactive species responsible for oxidative stress of *E. coli* when Ag/AgO/g-C_3N_4 photocatalyst is used.

Thus, the experimental results of AV-7 degradation and *E. coli* bacterial inactivation suggest that a synergistic combination of Ag, AgO and g-C_3N_4 can be a potential material for water purification processes.

4. Conclusions

Ag/AgO/g-CNMS photocatalyst is prepared successfully by a one step thermal method using silica as template. As prepared photocatalyst has lower band gap, reduced charge recombination and improved photocatalytic dye degradation (AV-7) performance compared to g-C_3N_4. The composite catalyst shows lower charge carrier resistance and better capacitive behavior compared to g-C_3N_4 as seen from the photoelectrochemical studies. The reaction pathway for the degradation of AV-7 dye is through the formation of intermediate species like dihydroxylated naphthalene, N-phenyl amide and hydrocarbon products. Additionally, this photocatalyst shows remarkable visible light induced inactivation of *E. coli* bacteria within 30 min of light irradiation. This composite catalyst has also shown a high thermal stability and reusability. The enhanced photocatalytic activity of the Ag/AgO/g-CNMS is attributed to a combined effect of enhanced light absorption and improved separation of charge carriers. Thus, the Ag/AgO/g-CNMS composite has the potential to emerge as a commercial photocatalyst for the degradation of acidic dyes and for the inactivation of bacteria.

Acknowledgements

The authors thank SAIF Shillong, Chandigarh and STIC cochin for their characterisation facility. D.V. acknowledge D. Krishnarao, School of chemistry, UoH for FESEM support. Prof. Dr. S.S.U acknowledge DST-SERB for financial assistance through project number SB/EMEQ-052/2014 SERB.

Appendix A. Supplementary data

Supplementary data associated with this article can be found, in the online version, at http://dx.doi.org/10.1016/j.apcatb.2017.09.030.

References

[1] C.-Y. Lin, D. Syrgabayeva, Asia Pacific Manag. Rev. (2016).
[2] W.-J. Ong, L.-L. Tan, Y.H. Ng, S.-T. Yong, S.-P. Chai, Chemicalreviews (2016).
[3] G. Liu, P. Niu, C. Sun, S.C. Smith, Z. Chen, G.Q. Lu, H.-M. Cheng, J. Am. Chem. Soc. 132 (2010) 11642–11648.
[4] J. Zhang, J. Sun, K. Maeda, K. Domen, P. Liu, M. Antonietti, X. Fu, X. Wang, Energy Environ. Sci. 4 (2011) 675–678.
[5] L. Ge, C. Han, X. Xiao, L. Guo, Y. Li, Mater. Res. Bull. 48 (2013) 3919–3925.
[6] J. Zhou, M. Zhang, Y. Zhu, Phys. Chem. Chem. Phys. 17 (2015) 3647–3652.
[7] X. Zhou, F. Peng, H. Wang, H. Yu, Y. Fang, Chem. Commun. 47 (2011) 10323–10325.
[8] Y. Wang, R. Shi, J. Lin, Y. Zhu, Energy Environ. Sci. 4 (2011) 2922–2929.
[9] L. Sun, X. Zhao, C.-J. Jia, Y. Zhou, X. Cheng, P. Li, L. Liu, W. Fan, J. Mater. Chem. 22 (2012) 23428–23438.
[10] X. Wang, S. Blechert, M. Antonietti, ACS Catal. 2 (2012) 1596–1606.
[11] L. Ge, F. Zuo, J. Liu, Q. Ma, C. Wang, D. Sun, L. Bartels, P. Feng, J. Phys. Chem. C 116 (2012) 13708–13714.
[12] X.-F. Gao, W.-T. Sun, Z.-D. Hu, G. Ai, Y.-L. Zhang, S. Feng, F. Li, L.-M. Peng, J. Phys. Chem. C 113 (2009) 20481–20485.
[13] S. Gawande, S.R. Thakare, ChemCatChem 4 (2012) 1759–1763.
[14] B. Subash, B. Krishnakumar, M. Swaminathan, M. Shanthi, Ind. Eng. Chem. Res. 53 (2014) 12953–12963.
[15] M. Xu, L. Han, S. Dong, Acs Appl Mater. Inter. 5 (2013) 12533–12540.
[16] K. Wu, Y. Cui, X. Wei, X. Song, J. Huang, J. Saudi Chem. Society 19 (2015) 465–470.
[17] H. Katsumata, T. Sakai, T. Suzuki, S. Kaneco, Ind. Eng. Chem. Res. 53 (2014) 8018–8025.
[18] S. Kumar, T. Surendar, A. Baruah, V. Shanker, J. Mater. Chem. A 1 (2013) 5333–5340.
[19] S. Wang, D. Li, C. Sun, S. Yang, Y. Guan, H. He, Appl. Catal. B: Environ. 144 (2014) 885–892.
[20] D. Jiang, L. Chen, J. Xie, M. Chen, Dalton Trans. 43 (2014) 4878–4885.
[21] A. Akhundi, A. Habibi-Yangjeh, Mater. Sci. Semicond. Process. 39 (2015) 162–171.
[22] Y. Li, Y. Zhao, L. Fang, R. Jin, Y. Yang, Y. Xing, Mater. Lett. 126 (2014) 5–8.
[23] L. Liu, Y. Qi, J. Yang, W. Cui, X. Li, Z. Zhang, Appl. Surf. Sci. Part A 358 (2015) 319–327.
[24] B.E. Breyfogle, C.J. Hung, M.G. Shumsky, J.A. Switzer, J. Electrochem. Soc. 143 (1996) 2741–2746.
[25] Y. Ida, S. Watase, T. Shinagawa, M. Watanabe, M. Chigane, M. Inaba, A. Tasaka, M. Izaki, Chem. Mater. 20 (2008) 1254–1256.
[26] A.J. Varkey, A.F. Fort, Sol. Energy Mater. Sol. Cells 29 (1993) 253–259.
[27] M.J. Bojdys, J.O. Müller, M. Antonietti, A. Thomas, Chem.–A Euro. J. 14 (2008) 8177–8182.
[28] K. Tian, W.-J. Liu, H. Jiang, ACS Sustain. Chem. Eng. 3 (2015) 269–276.
[29] Q. Lv, C. Cao, C. Li, J. Zhang, H. Zhu, X. Kong, X. Duan, J. Mater. Chem. 13 (2003) 1241–1243.
[30] C.-B. Cao, Q. Lv, H.-S. Zhu, Diamond Relat. Mater. 12 (2003) 1070–1074.
[31] E.G. Gillan, Chem. Mater. 12 (2000) 3906–3912.
[32] P. Zhang, X. Li, C. Shao, Y. Liu, J. Mater. Chem. A 3 (2015) 3281–3284.
[33] S. Fu, Y. He, Q. Wu, Y. Wu, T. Wu, J. Mater. Res. 31 (2016) 2252–2260.
[34] M. Jabłońska, M. Nocuń, E. Bidzińska, Catal. Lett. 146 (2016) 937–944.
[35] J.F. Weaver, G.B. Hoflund, J. Phys. Chem. 98 (1994) 8519–8524.
[36] G. Zhang, G. Li, X. Wang, Chemcatchem 7 (2015) 2864–2870.
[37] Y. Kang, Y. Yang, L.-C. Yin, X. Kang, G. Liu, H.-M. Cheng, Adv. Mater. 27 (2015) 4572–4577.
[38] J. Deng, J. Liang, M. Li, M. Tong, Colloids Surf. B: Biointerfaces 152 (2017) 49–57.
[39] J. Liu, T. Zhang, Z. Wang, G. Dawson, W. Chen, J. Mater. Chem. 21 (2011) 14398–14401.
[40] Y.-S. Xu, W.-D. Zhang, ChemCatChem 5 (2013) 2343–2351.
[41] F. Chen, Q. Yang, Y. Wang, J. Zhao, D. Wang, X. Li, Z. Guo, H. Wang, Y. Deng, C. Niu, G. Zeng, Appl. Catal. B: Environ. 205 (2017) 133–147.
[42] P. Wang, B. Huang, X. Qin, X. Zhang, Y. Dai, J. Wei, M.-H. Whangbo, Angew. Chem. Int. Ed. 47 (2008) 7931–7933.
[43] X. Zhang, Y. Wang, F. Hou, H. Li, Y. Yang, X. Zhang, Y. Yang, Y. Wang, Appl. Surf. Sci. Part B 391 (2017) 476–483.
[44] F. Fabregat-Santiago, G. Garcia-Belmonte, I. Mora-Seró, J. Bisquert, Phys. Chem. Chem. Phys. 13 (2011) 9083.
[45] Y. Zhang, J. Wang, P. Wan, J. Ye, S. Hussain, H. Wei, D. Hou, Mater. Lett. 177 (2016) 71–75.
[46] X.F. Li, J. Zhang, L.H. Shen, Y.M. Ma, W.W. Lei, Q.L. Cui, G.T. Zou, Appl. Phys. A-Mater. 94 (2009) 387–392.
[47] U.G. Akpan, B.H. Hameed, J. Hazard. Mater. 170 (2009) 520–529.
[48] R. Vinu, G. Madras, J. Indian Inst. Sci. 90 (2012) 189–230.
[49] D.T. Sawyer, J.S. Valentine, Acc. Chem. Res. 14 (1981) 393–400.
[50] A. Kudo, Y. Miseki, Chem. Soc. Rev. 38 (2009) 253–278.
[51] S.A. Ansari, M.O. Ansari, M.H. Cho, Sci. Rep.-Uk 6 (2016) 27713.
[52] P. Christopher, H. Xin, S. Linic, Nat. Chem. 3 (2011) 467–472.
[53] L. Shi, L. Liang, J. Ma, F. Wang, J. Sun, Catal. Sci. Technol. 4 (2014) 758–765.